Contributions to Mineralogy and Petrology (2022) 177:62
https://doi.org/10.1007/s00410-022-01930-9

ORIGINAL PAPER

Long-lived dacitic magmatic systems and recharge dynamics in the Jemez Mountains volcanic field, western USA

Jie Wu[1] · Michael C. Rowe[1] · Shane J. Cronin[1] · John A. Wolff[2] · Bin Fu[3]

Received: 20 May 2021 / Accepted: 6 June 2022 / Published online: 18 June 2022

Abstract

We examine the connected history of dacite-dominant volcanic rocks of the Tschicoma Formation, erupted between 5.5 and 2 Ma from the Jemez Mountains volcanic field, western USA. Zircon samples from two separate eruptions have continuous SHRIMP U–Pb age spectra spanning 0.84–1.08 Myr duration (3.12–3.96 Ma and 3.50–4.58 Ma, respectively), following an episode of zircon crystallization 0.28–0.50 Myr earlier (at 4.46 Ma and 4.86 Ma, respectively). Zircon chemical variations, as well as ubiquitous resorption textures that commonly show large core-rim age differences (up to 720–740 kyr), suggest that they grew in separate melt lenses. Zircons were likely stored at near-solidus or even sub-solidus conditions after crystallization, but may have been reactivated in response to at least four major magma recharge events every 300–400 kyr and smaller events in between. A cycle of zircon dissolution (from heating), recrystallization (during cooling), and storage repeated in different locations in the Tschicoma mush system throughout its lifespan; each recharge-induced heating stage may last for several hundred to more than a thousand years based on calculations of zircon dissolution. We envisage the melt lenses to be distributed in a crystal mush zone, coalescing into a single magma batch as magma recharge occurs shortly before eruption. Once active, increasing magma supply rates may trigger large-scale partial melting of the pre-existing mush and caldera-forming eruptions.

Keywords Zircon age · Geochemistry · Dacite · Magmatic system · Silicic mush

Introduction

With the potential to survive magmatic re-entrainment while preserving its original age and composition, zircon is considered the most useful petrologic tool to reveal magma longevity and assembly history (Hawkesworth and Kemp 2006; Siebel et al. 2009; Walker et al. 2010). Large volcanic systems in the shallow crust are frequently found to have lifespans > 100 ky, based on zircon age variation (e.g., Whakamaru ignimbrite, Brown and Fletcher 1999; young rhyolitic systems at Long Valley, Reid et al. 1997; the Youngest Toba Tuff, Reid and Vazquez 2017). In some cases, continuous zircon age spectra can be as large as 1–2 Myr for both incrementally grown plutonic systems (e.g., Spirit Mountain batholith, Walker et al. 2007) and intermediate-to-silicic volcanic systems (e.g., the Aucanquilcha volcanic cluster, Walker et al. 2010; Timber Mountain complex, Bindeman et al. 2006; Kneeling Nun Tuff, Szymanowski et al. 2019; Chuhuilla and Pastos Grandes Ignimbrites, Kaiser 2014, Kaiser et al. 2017). Prolonged magma storage can be explained using a mixed crystal-melt mush model (Bachmann and Bergantz 2004; Cashman et al. 2017), since a partially molten state of magma may be more thermally efficient to maintain than a melt-dominated magma chamber (Karakas and Dufek 2015; Cashman et al. 2017). Such a long-lived magma reservoir can be stored at near-solidus conditions for most its lifespan and punctuated by rejuvenation as long as magma supply rates are sufficient to keep the system operating (e.g., Cooper and Kent 2014; Rubin et al. 2017; Szymanowski et al. 2017; Kent and Cooper 2018). In the present study, we use zircon geochronology

Communicated by Gordon Moore.

✉ Jie Wu
jie.wu@auckland.ac.nz

[1] School of Environment, The University of Auckland, Auckland 1142, New Zealand

[2] School of the Environment, Washington State University, Pullman, WA 99164, USA

[3] Research School of Earth Sciences, Australian National University, Canberra, ACT 2601, Australia

and compositions to unravel the construction, evolution, and persistence of a long-lived magmatic system.

The Jemez Mountains volcanic field (JMVF) in north-central New Mexico is located at the junction of the Rio Grande rift and the Jemez lineament, a Neoproterozoic subduction-induced suture (Shaw and Karlstrom 1999; Karlstrom et al. 2002). Major construction of the JMVF started at ~ 10 Ma (Fig. 1; Gardner et al. 1986; WoldeGabriel et al. 2007; Kelley et al. 2013), upon a substrate of Paleozoic sedimentary rocks and Proterozoic basement (Smith et al. 1970; Brookins and Laughlin 1983). Early erupted products from 10 to 6 Ma varied from basaltic to rhyolitic lavas, dominated by the ~ 1000 km^3 andesite-dominant intermediate composition Paliza Canyon Formation. After a 0.5 Myr hiatus, renewed volcanic eruptions occurred in the northern and eastern JMVF, volumetrically dominated by the dacite-dominant intermediate-to-silicic Tschicoma Formation (~ 500 km^3) that erupted between 5.5 and 2 Ma (Gardner et al. 1986; Kelley et al. 2013). This new stage of volcanism corresponded to reactivation of local tectonic activity that shifted eastward from the Cañada de Cochiti fault zone to the Pajarito fault zone at 5–4 Ma (Fig. 1; Gardner and Goff 1984). The later stages of Tschicoma activity are accompanied by eruptions of mafic lavas in peripheral areas (the Cerros del Rio and El Alto basaltic fields). Following small-scale rhyolitic eruptions at ~ 1.85 Ma, which are thought to represent early magma leakage from the large Bandelier system, two episodes of caldera-forming eruptions at 1.60 and 1.25 Ma, respectively, produced the voluminous Otowi and Tshirege members of the Bandelier Tuff (a dense rock equivalent magma volume of ~ 400 km^3 each; Phillips et al. 2007; Gardner et al. 2010; Goff et al. 2014; Wolff and Ramos 2014; Cook et al. 2016).

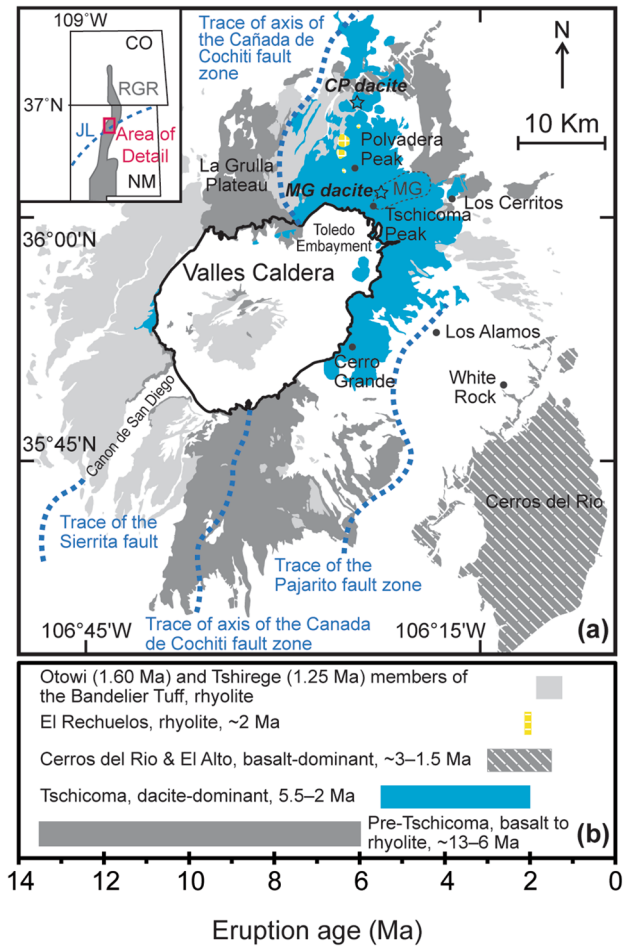

Fig. 1 Geological map of the Jemez Mountains volcanic field (**a**, modified after Smith et al. 1970; Aldrich 1986; Wolff et al. 2005; Rowe et al. 2007; Wu et al. 2020) and stratigraphic column (**b**) showing temporal ranges of geological units in **a**. Stars mark the sampling locations. Inset: the Rio Grande rift (RGR) and Jemez lineament (JL, dashed blue line) in Colorado and New Mexico, showing location of the study area. *CP* Cerro Pelón (east), *MG* Mesa de la Gallina

This study focuses on the Tschicoma Formation lavas erupted during ~ 5–2 Ma (Kelley et al. 2013), covering an area of ~ 911 km^2 (estimated based on the surface exposure in Fig. 1). Domes and lava flows formed via at least 19 identified vents (Smith et al. 1970) in the northeast and east areas, adding up to a total volume of ~ 500 km^3 (Gardner et al. 1986). Exposure of Tschicoma rocks on the western caldera rim (Fig. 1) indicates that Tschicoma magmas likely also erupted in the central field, but their vents and flows were destroyed and overprinted by the two super-scale caldera-forming events. Tschicoma lavas are dominantly dacitic domes and coulées, with subordinate andesite and rhyolite.

Magma mixing occurred during Tschicoma petrogenesis based on both whole-rock geochemistry (Rowe et al. 2007), and mineral texture and chemistry (Wu et al. 2020). From whole-rock geochemistry, Rowe et al. (2007) modelled the chemical variability of the Tschicoma Formation as a simple mixture between basaltic andesite, represented by mafic enclaves within the dacites from northeast field, and a silicic crustal endmember (represented by Otowi granitoid lithic fragments). Wu et al. (2020) carried out a detailed chemical and textural study on major mineral phases (including plagioclase and amphibole) from the Tschicoma dacites, suggesting a more complex magma evolution with three mafic endmembers and one silicic endmember. Plagioclase with disequilibrium textures (e.g., patchy-core and sieved-rim) commonly has a Ca-poor core and Ca-rich rim, consistent with magma mixing/recharge, while two groups of amphibole, characterized by low-Al and high-Al compositions, indicate low- and high-temperature crystallization, respectively. Based on mineral trace-element data, Wu et al. (2020) concluded that the Ca-poor plagioclase and low-Al, low-temperature amphibole were crystallized in an upper crustal silicic mush that was frequently recharged by less-evolved magmas from middle-lower crust.

As a reliable geochronometer, zircon is also a host for a range of trace elements (including rare-earth elements), and variations in zircon trace elements reflect changes in compositions of its host melt. We hypothesize that zircons from the Tschicoma dacites have large age spectra similar to the previously mentioned long-lived magmatic systems (e.g., the Aucanquilcha volcanic cluster), and thus record age-constrained compositional changes throughout the lifetime of this upper crustal silicic mush zone. Therefore, we conducted age dating, trace element, and O-isotopic analyses, on zircons from the Tschicoma dacites to test if the magma recharge and mixing events identified by Wu et al (2020) are recorded in Tschicoma zircons and to understand the assembly and persistence of the pre-caldera silicic magma reservoir. For this study, two Tschicoma dacite samples were collected from the Mesa de la Gallina lava flow (sample JWJM16-4 with 67.93 wt% SiO_2 on an anhydrous basis) erupted from the Tschicoma Peak and the Cerro Pelón (east) Dome (sample JWJM16-5 with 67.38 wt% SiO_2 on an anhydrous basis), referred to as MG dacite and CP dacite, respectively (Fig. 1; see Table S1 in Supplementary Appendix for the whole-rock compositions). The two sampling sites are in northeast JMVF, the area where most surviving Tschicoma rocks are located. Both samples are porphyritic (41–43 vol% crystallinity) and the major mineral phases are plagioclase (22.9–29.1 vol%), clinopyroxene (4.3–8.9 vol%), orthopyroxene (4.5–4.9 vol%), and amphibole (4.4–4.8 vol%). Minor biotite and alkali feldspar are observed only in the CP dacite. These samples were chosen based on whole-rock chemistry (Rowe et al. 2007) indicating zircon saturation. The vents from which they were erupted are located ~ 12 km apart so likely represent separate parts of the magmatic system, or individual systems. Previous $^{40}Ar/^{39}Ar$ dating shows that the CP Dome (3.64 ± 0.03 Ma) formed later than the MG lavas that range in age from 3.66 ± 0.09 to 4.49 ± 0.15 Ma (Kelley et al. 2013).

Methods

Sample preparation

The two Tschicoma samples were cleaned and crushed into coarse powders using a jaw crusher followed by a disk mill. The crushed samples went through a Gemini table utilizing water flow and vibration to remove light minerals (e.g., plagioclase) and matrix. The reduced samples were subsequently separated into four different size fractions (> 250 µm, 250–150 µm, 150–60 µm, and < 60 µm) by wet sieving. Samples in the size fractions of 250–150 µm and 150–60 µm were processed by heavy liquid separation using LST heavy liquid with density of 2.85 g/ml. Ferromagnetic minerals (e.g., magnetite) were manually removed with a hand-magnet, after which paramagnetic minerals (e.g., pyroxene and amphibole) were removed using a Frantz magnetic separator. Finally, zircon crystals were hand-picked under binocular microscope. Separated zircon grains were mounted with standard zircon Temora-2 at Australian National University (ANU). In total, 189 zircon grains (33 of size 250–150 µm and 156 of size 150–60 µm) from sample JWJM16-4, and 210 grains (43 of size 250–150 µm and 167 of size 150–60 µm) from sample JWJM16-5 were mounted and ground to expose interior. Zircon cathodoluminescence (CL) images were taken using Scanning Electron Microscopy (SEM) at Victoria University of Wellington to reveal textural details. Based on the CL images, representative zircon grains were sequentially analysed for U–Pb age dating, oxygen isotope ratios, and trace-element concentrations. The three types of analyses were conducted at the same locations with a slight polish to remove the U–Pb SHRIMP pits before the O-isotopic analyses. Zircons with resorbed cores and overgrowth of new rims potentially record multiple growth events, and they are thus the main target for analyses on both core and rim. All data are initially reported by Wu et al. (2021) and shown in Supplementary Table S2.

Zircon U–Pb dating

Zircon samples were analysed for U–Pb isotope ratios with SHRIMP II at ANU, with a spot size of ~ 25 µm and primary O_2^- beam mainly between 5 and 6 nA. During the analyses, Temora-2 reference zircon was analysed after each two or three unknown zircon grains. The U–Pb data were corrected for common Pb using the measured $^{238}U/^{206}Pb$ and $^{207}Pb/^{206}Pb$ ratios following Tera and Wasserburg (1972) as outlined in Williams (1998). The final U–Pb ages were corrected for initial ^{234}U–^{230}Th disequilibrium using corresponding whole-rock Th/U ratios (data from Wu et al. 2020) following Schärer (1984). Pb loss is unlikely in the MG and CP zircons for the following reasons: (1) most zircon data are either on or close to the concordia curve in the Tera–Wasserburg (T–W) diagram (Fig. S1 in Supplementary Appendix); (2) the volume diffusion rate of Pb in crystalline zircon crystal is extremely slow at crustal conditions (e.g., $D = 1.1$ µm^2/Myr at $T = 900$ °C, Cherniak and Watson 2001), and the MG and CP zircons are large (a length of ~ 140–480 µm) crystals that are hosted in fresh lavas younger than 5 Ma.

Zircon oxygen isotopes

After U–Pb dating, the zircon samples were analysed for O-isotopic compositions using the SHRIMP SI at ANU, with a spot size of ~ 25 µm. During the analytical session, reference zircons FC-1 and Temora-2 were used as calibration and internal standards, respectively. Corrected $^{18}O/^{16}O$

ratios are reported in $\delta^{18}O$ notation, in permil variations relative to Vienna standard mean ocean water (VSMOW). $\delta^{18}O = \{(^{18}O/^{16}O)_{sample}/(^{18}O/^{16}O)_{VSMOW} - 1\} \times 1000$, and $(^{18}O/^{16}O)_{VSMOW} = 0.0020052$. All $\delta^{18}O$ values were calibrated against standard zircon FC-1 [5.61 ± 0.14‰, 2σ, $N = 6$ (J.W. Valley, unpublished data); see Fu et al. 2015]. The spot-to-spot reproducibility (external precision) was typically better than ± 0.50‰ (2σ). Average $\delta^{18}O$ for Temora-2 zircon, 7.98‰, is within analytical uncertainty to the accepted value, 8.20‰ (Valley 2003; Black et al. 2004).

Zircon trace elements

After zircon O-isotope analyses, zircon grains were analysed for trace-element concentrations using an Agilent 7700 s-lens ICP-MS coupled with an ESI/NWR 193 ArF excimer laser at the University of Auckland. Synthetic reference glasses GSE-1G and GSD-1G (Jochum et al. 2005) were used as primary and secondary standards respectively, both analysed after every ten unknowns. The analyses were conducted with an ablation size of 55 µm. Compared to SHRIMP analyses, the larger spot size during laser ablation means more zones were averaged in some texturally complex zircon grains. Data were collected during 60 s of ablation time with rep rate of 5 Hz and laser energy ~ 8 J/cm^2. The final data were internally normalized using ^{29}Si and GSE-1G as a calibration standard. The 1SD values of repeated analysis of secondary standards (GSD-1G) are 7.0% relative for Hf and 2.7–5.4% relative for Ti, Sr, Nb, Ta, Y, and REE.

Results

Zircon texture

Zircon crystals are morphologically and texturally similar between the two dacites. Zircon grains are transparent, or occasionally brown coloured, and are all rich in inclusions (Fig. 2). Most grains are short-to-long prisms with a length of ~ 140–480 µm, a width of ~ 60–240 µm, and an aspect ratio (length:width) of 1.5–4.9 (average of 2.4 with 1σ of 0.5). In contrast to magmatic zircons that usually have flat surfaces and sharp edges, many Tschicoma zircon crystals are somewhat rounded, which indicates crystal resorption before eruption (Fig. 2). Zircon CL images reveal complex zoning patterns (Fig. 2 and Supplementary Fig. S2). Obvious textural differences between cores and rims are observed in most zircon grains. Zircon cores are dominantly sector zoned and sometimes can be patchy or homogenous, and rims are commonly oscillatory or sector zoned. A single resorbed surface is commonly observed between cores and rims (27% of CL imaged zircon grains); multiple resorptions were not evident.

Zircon U–Pb age

Although zircons from the MG dacite record systematically older ages than those from the CP dacite (3.50–4.86 Ma and 3.12–4.46 Ma, respectively), zircons from both samples have continuous age spectra of ~ 1 Myr duration (3.50–4.58 Ma and 3.12–3.96 Ma for MG and CP zircons, respectively), following the first zircon growth events that are 0.28–0.50 Myr older (at 4.86 Ma and 4.46 Ma for MG and CP zircons, respectively) (Fig. 3). The 1σ age uncertainties range from 50 to 160 kyr, with an average of 90 kyr. Zircon from the MG dacite shows a relatively uniform age distribution, while that of the CP dacite is skewed toward younger populations. In both samples, zircon cores and rims have similar age spans, which are 3.50–4.86 Ma (core) and 3.53–4.55 Ma (rim) for the MG zircons, and 3.21–4.46 Ma (core) and 3.12–3.72 Ma (rim) for the CP zircons (Fig. 3). Core and rim analyses on the same zircon grains tend to show age differences. A total of 13 out of 19 zircon core-rim pairs from the MG dacite and 6 out of 9 zircon core-rim pairs from the CP dacite have old cores and young rims with age difference much larger than analytical uncertainty (140–280 kyr, sum of 1σ uncertainties of cores and corresponding rims; Fig. 4), up to 720–740 kyr in both samples. Protracted zircon crystallization over timescales well outside the bounds of analytical uncertainties means a weighted average age (4.10 ± 0.09 Ma, N = 48 and 3.50 ± 0.09 Ma, N = 39 for MG and CP zircons, respectively, 95% confidence) does not appropriately describe the complexities of the data, which is evident from the corresponding very large mean square of weighted deviation (MSWD = 12 and 14, respectively; Kaiser et al. 2017). Here, we calculate the average age of the youngest zircon grain clusters at 1σ uncertainty (e.g., Coutts et al. 2019). The calculated age for the MG dacite (3.59 ± 0.10 Ma, MSWD = 0.74, $N = 4$, 95% confidence) agrees with the $^{40}Ar/^{39}Ar$ eruption age (from 3.66 ± 0.09 to 4.49 ± 0.15 Ma, Kelley et al. 2013). However, the age for the CP dacite (3.21 ± 0.05 Ma, MSWD = 0.41, $N = 10$, 95% confidence) postdates the reported $^{40}Ar/^{39}Ar$ age (3.64 ± 0.03 Ma, Kelley et al. 2013), but is consistent with the K–Ar age (2.96 ± 0.27 Ma, Goff et al. 1989). Therefore, the eruption ages for MG and CP dacites can be approximated by the average age of the youngest zircon grain clusters at 1σ uncertainty.

Zircon O-isotopes and trace elements

Fractionation of O-isotopes between melt and zircon ($\Delta^{18}O_{melt\text{-}zircon}$) is controlled by melt composition and temperature; we use $\delta^{18}O_{zircon}$ and $\delta^{18}O_{melt}$ to denote $\delta^{18}O$ values for zircon and its host melt, respectively. Here, we calculate O-isotopic compositions of melt in equilibrium with zircon following the calibration of Qin et al. (2016) using calculated melt compositions and the average zircon crystallization

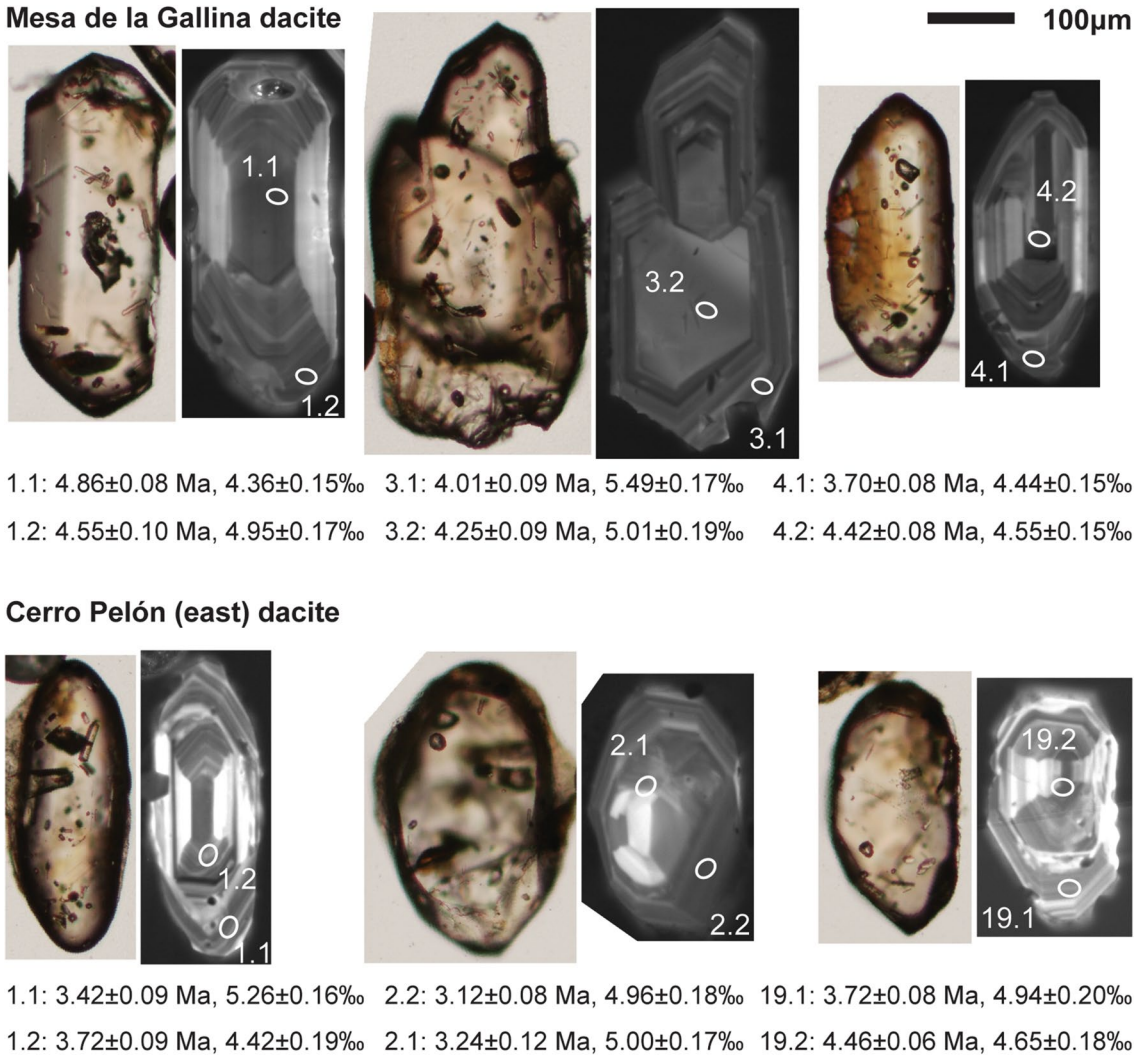

Fig. 2 Cathodoluminescence (CL) and plane polarized light (ppl) images of selected zircons from the two Tschicoma dacites. White ellipses labelled with analysis number mark location for both U–Pb age and oxygen isotope analyses. Note that trace-element concentrations were analysed at the same location as the SHRIMP pits, but with a larger spot size (55 vs 25 μm). Zircon age (Ma) followed by $\delta^{18}O_{zircon}$ (‰, VSMOW) is shown after the analysis number, with 1σ uncertainty shown

temperatures ($T_{Ti\text{-}in\text{-}zircon}$, calculated after Ferry and Watson 2007). $T_{Ti\text{-}in\text{-}zircon}$ is calculated with $a_{SiO2} = 1.0$ (small quartz grains are present in the matrix) and $a_{TiO2} = 0.78$ (see Supplementary Table S2 for results); the a_{TiO2} value is based on compositions of equilibrium Fe–Ti oxide pairs (Wu et al. 2020). We note that the selected a_{TiO2} value based on Fe–Ti oxide pairs likely reflects conditions for magma immediately before eruption rather than magma in equilibrium with zircon (Hou et al. 2020). However, an analysis of sensitivity shows that a decrease of 0.2 in a_{TiO2} value only results in an average temperate increase of 28 °C, which is smaller than the uncertainty of the thermometer itself (average of 35 °C). We use an average temperature for the calculation, as a 50 °C temperature increase only results in a decrease of ~ 0.1‰ in $\Delta^{18}O_{melt\text{-}zircon}$ value. We also note that the whole-rock composition is unlikely to represent the melt in equilibrium with the MG and CP zircons, given that MG and CP dacites are crystal-rich and the zircons crystallized over a timespan of ~ 1 Myr. Major-element compositions for melt in equilibrium with Tschicoma zircons are calculated by subtracting major mineral phases from the whole-rock compositions by mass balance (detailed calculations and results are available in Supplementary Appendix). Volumetric percentages of minerals are based on point-counting on thin sections, and major-element compositions for plagioclase, pyroxene, and amphibole are averages based on electron microprobe analysis (EMPA data from Wu et al. 2020). The calculated melts are rhyolitic in composition for both samples (75 and 73 wt% SiO_2 for MG and CP samples, respectively; Supplementary Table S1). Using calculated melt major compositions

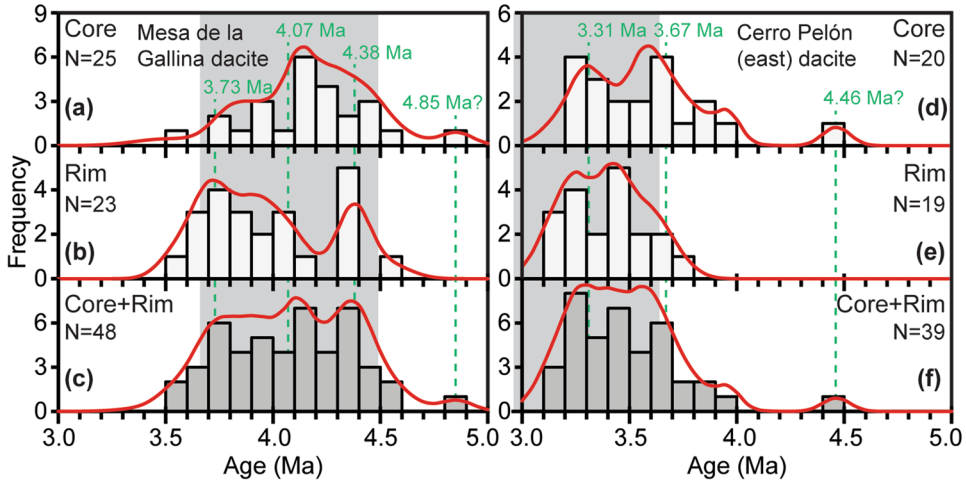

Fig. 3 Histogram of the age distribution for zircon cores (**a** and **d**), rims (**b** and **e**) and a combination of both (**c** and **f**) from the two Tschicoma dacites with probability density function (PDF) curves shown. The average 1σ uncertainty (90 kyr) is close to the bin width. PDF is calculated as a sum of normal distributions of all individual age analyses. Individual episodes of zircon growth identified by age unmixing calculations are marked with green dashed lines. Grey shades in the background are the ranges of Ar–Ar and K–Ar ages (3.66–4.49 Ma and 2.96–3.64 Ma for MG and CP dacites, respectively) from Kelley et al. (2013) and Goff et al. (1989)

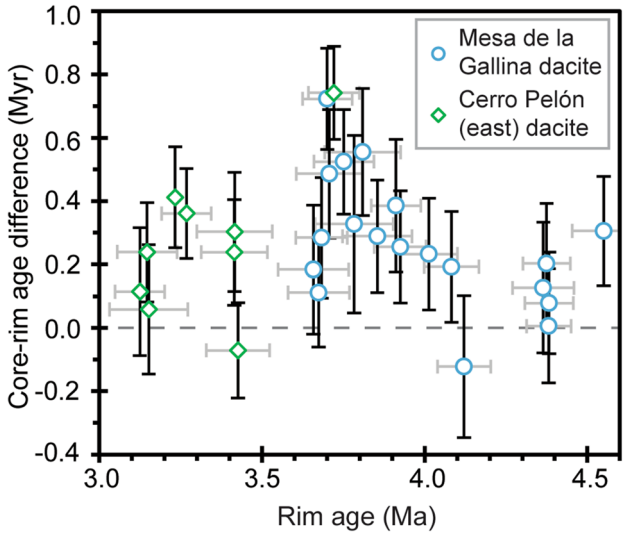

Fig. 4 Zircon age difference between cores and rims in individual grains from the two Tschicoma dacites. The vertical error bar represents the sum of 2σ uncertainties of core and rim, and the horizontal error bar is the 2σ uncertainty for zircon rim age

and whole-rock Zr concentration, the calculated zircon saturation temperature based on Watson and Harrison (1983) is ~ 780 °C, which is higher than the weighted average $T_{\text{Ti-in-zircon}}$ at ~ 730 °C, although the model of Boehnke et al. (2013) gives a lower zircon saturation temperature at ~ 730 °C. Tschicoma zircons may have crystallized from a range of melt compositions, given their diversity in chemical compositions. Calculation of $\Delta^{18}O_{\text{melt-zircon}}$ using the MG and CP whole-rock compositions (67.93 and 67.38 wt% SiO_2, respectively) decreases the $\Delta^{18}O_{\text{melt-zircon}}$ value by 0.26–0.27‰. Those uncertainties are relatively small when compared to the large $\delta^{18}O$ variation (1.73‰, excluding two extremely high and low values) in the Tschicoma zircons. We also compare $\delta^{18}O$ between Tschicoma zircons and those from two pre-Tschicoma units (Paliza Canyon low-Si dacite and Bearhead rhyolite; whole-rock data are available in Supplementary Table S1) in a later section. For $\Delta^{18}O_{\text{melt-zircon}}$ calculation, Paliza Canyon melt compositions are also calculated by mass balance removal of major mineral phases from whole-rock compositions; the $\Delta^{18}O_{\text{melt-zircon}}$ value increases only by 0.13‰ when compared to the result based on Paliza Canyon whole-rock composition. For the Bearhead rhyolite, we simply used the whole-rock composition to calculate $\Delta^{18}O_{\text{melt-zircon}}$ given its low crystal content (10 vol%). Calculated $\Delta^{18}O_{\text{melt-zircon}}$ values based on different melt compositions are available in Supplementary Appendix. Zircons from both Tschicoma samples show similar large but continuous $\delta^{18}O_{\text{melt}}$ variations (5.84–7.37‰ and 5.99–7.56‰ for MG and CP samples, respectively), except for two extremely high (8.23‰) and low (5.05‰) calculated $\delta^{18}O_{\text{melt}}$ values recorded in zircon cores from the MG dacite (Fig. 5a). Both samples have similar $\delta^{18}O_{\text{melt}}$ PDF curve peaks above the normal-$\delta^{18}O$ range (mantle differentiation array, ranging from 5.8 ± 0.2‰ for parent mantle basalts to 6.1 ± 0.3‰ for their resulting rhyolites at ~ 90% fractional crystallization; Bindeman et al. 2004), while the MG dacite has a small shoulder at normal mantle range (Fig. 5a). Both the MG and CP dacites yield similar weighted average zircon-derived $\delta^{18}O_{\text{melt}}$ values (6.72 ± 0.51‰ and 6.79 ± 0.37‰, respectively; 1σ uncertainty). Though both zircon cores and rims

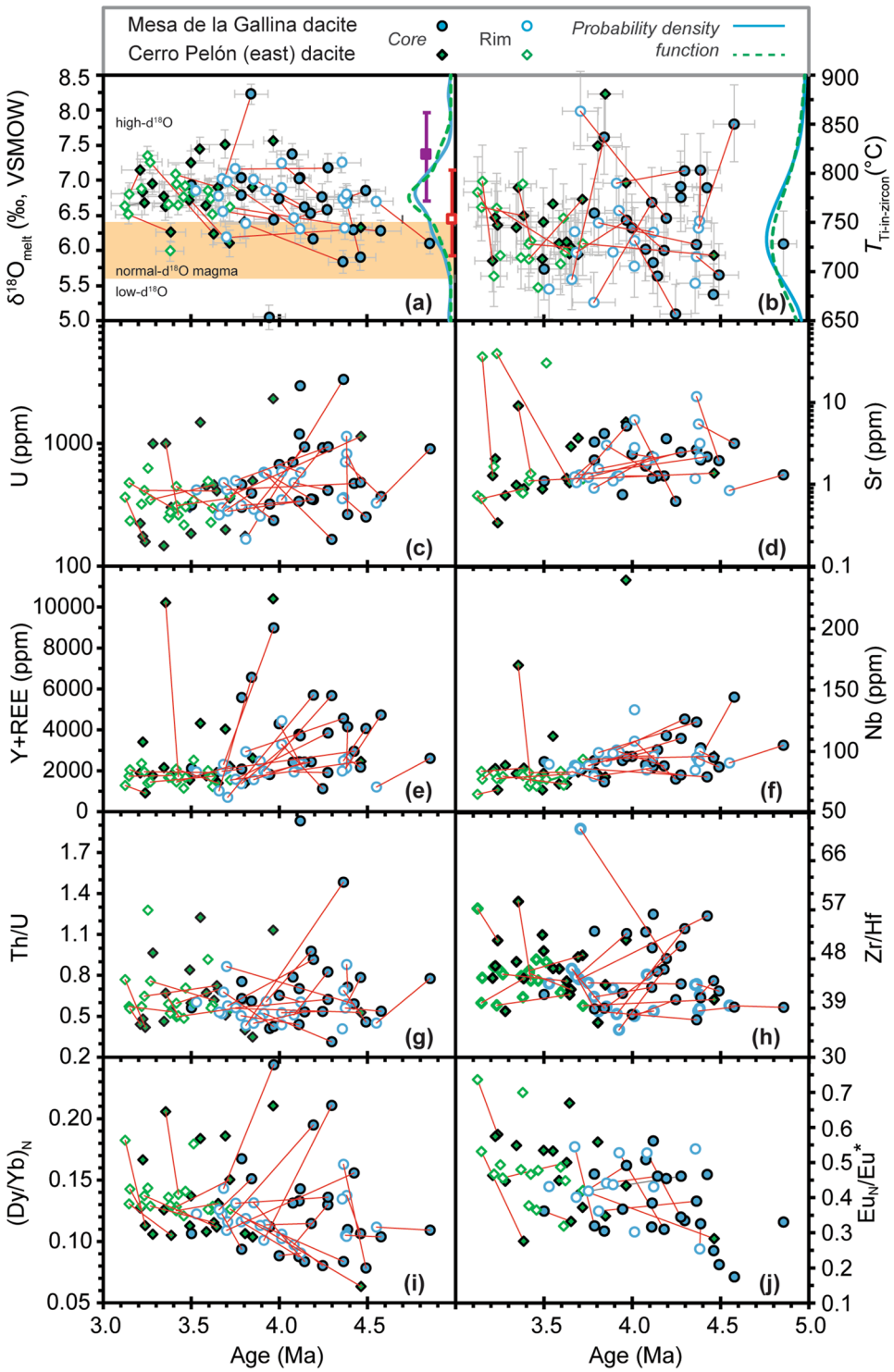

Fig. 5 Variation of zircon composition with U–Pb age, including calculated zircon-derived $\delta^{18}O_{melt}$ (**a**), crystallization temperature (**b**), trace-element concentrations (**c**–**f**), element ratios (**g**–**i**), and Eu_N/Eu^* (**j**). Probability density function (PDF) curves of $\delta^{18}O_{melt}$ and temperature for each sample are also shown in **a** and **b**. Normal-$\delta^{18}O$ magma range is based on the mantle differentiation array (from 5.8 ± 0.2 to 6.1 ± 0.3‰) of Bindeman et al. (2004). Tie lines connect core and rim analyses from individual grains where both core and rim analyses are available. Filled purple and open red squares in panel **a** are the average zircon-derived $\delta^{18}O_{melt}$ values for the Bearhead and Paliza Canyon formations, respectively, and the corresponding bars represent the whole $\delta^{18}O_{melt}$ range (data from Wu et al. 2021). 2σ error bars for trace elements are smaller than the symbols and thus are not shown

record similar large variations in $\delta^{18}O_{melt}$, most core and rim analyses on the same grains show rim-ward increases in both samples (17 out of 25 zircon core-rim pairs; Fig. 5a and 6a).

Trace-element concentrations in Tschicoma zircons show large variations and do not follow obvious broad patterns (Figs. 5 and 6). Contemporaneous zircon grains (with ages overlapping within 1σ uncertainty) from the MG and CP samples have similar trace-element compositions, and thus, all zircon grains form a continuum in the composition-age space. Trace-element outliers are defined as greater than 2σ of the mean and are excluded in the following comparison between MG and CP zircon compositions. Compared to the zircons from the CP dacite, those from the MG dacite have similar ranges in Ti (which is used for calculation of

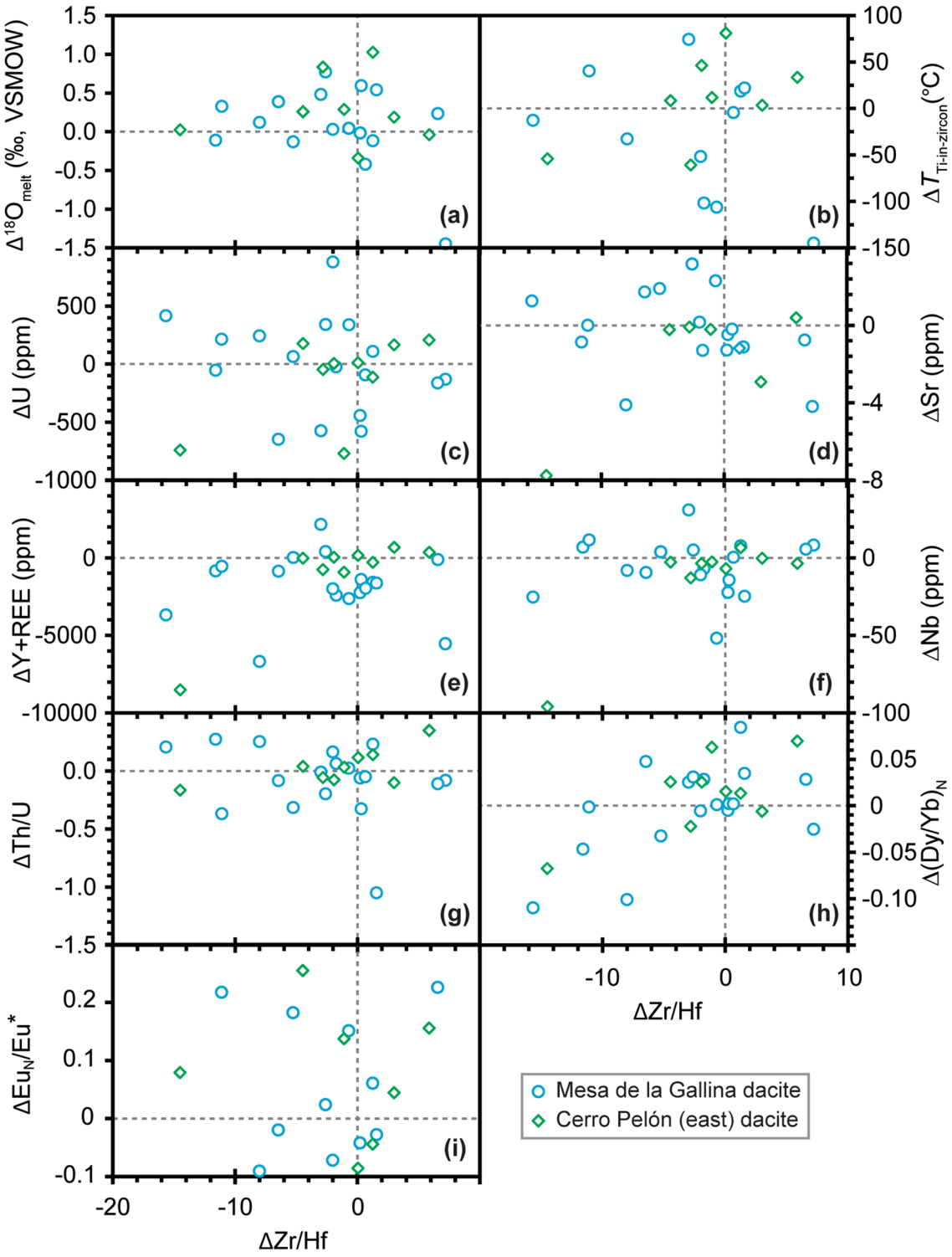

Fig. 6 Rim-ward compositional variations with ΔZr/Hf in individual zircon grains from the two Tschicoma dacites, including zircon-derived $\delta^{18}O_{melt}$ (**a**), crystallization temperature (**b**), trace-element concentrations (**c**–**f**), element ratios (**g** and **h**), and Eu_N/Eu^* (**i**). The symbol Δ represents compositional difference between rim and core (i.e., Δ = rim-core). $\Delta^{18}O_{melt} = \delta^{18}O_{melt}$ (rim)-$\delta^{18}O_{melt}$ (core)

zircon crystallization temperature, $T_{Ti\text{-}in\text{-}zircon}$; 657–803 vs 684–790 °C), U (165–1192 vs 147–1144 ppm), Sr (0.62–3.61 vs 0.34–3.67 ppm), Th/U (0.31–0.98 vs 0.35–0.96), Zr/Hf (35–54 vs 36–52) and $(Dy/Yb)_N$ (0.08–0.19 vs 0.10–0.19, where *N* is normalization to chondrite values after Sun and McDonough 1989), slightly less Eu anomalies (Eu_N/Eu^*,

where $Eu^* = \sqrt{(Sm_N \times Gd_N)}$, N denotes chondrite normalized; 0.21–0.56 vs 0.28–0.67), but larger overall and core-rim variations in Y + REE (1023–5694 vs 917–4322 ppm) and Nb (75–124 vs 65–112 ppm). Both samples have a crystallization temperature ($T_{\text{Ti-in-zircon}}$) mode centered at ~ 730 °C. In the MG dacite, zircon cores generally show larger chemical variations than rims. There are notable rimward decreases in Y + REE (20 out of 27 zircon core-rim pairs) and Nb (17 out of 27 pairs), as well as increases in Eu anomaly (11 out of 18 pairs), correlating overall with U–Pb ages. Core-rim variations in other trace elements do not follow any consistent pattern.

Discussion

History of zircon growth

Zircon grains from the two samples have similar PDF curves of age distribution, characterized by relatively flat distribution during 3.7–4.4 Ma (MG) and 3.2–3.6 Ma (CP) without notable peaks (Fig. 3c and f). The extremely high MSWD values (> 10) for each sample indicate zircon crystallization over a time period that far exceeds the analytical uncertainties, with average ages not reflecting the complexities of the age populations. To determine how many zircon populations are needed to explain each age spectrum, we use the age unmixing algorithm of Sambridge and Compston (1994) as implemented in Isoplot (Ludwig 2008). The results suggest three (at 3.31 ± 0.02, 3.67 ± 0.02, and 4.46 ± 0.07 Ma, 1σ uncertainty; with a proportion of 57%, 40%, and 3%, respectively, and a relative misfit value of 0.060; CP zircons) and four (at 3.73 ± 0.04, 4.07 ± 0.03, 4.38 ± 0.02 and 4.85 ± 0.08 Ma, 1σ uncertainty; with a proportion of 31%, 33%, 33% and 2%, respectively, and a relative misfit value of 0.033; MG zircons) normally distributed sub-groups best explain the whole zircon populations; a further increase of components does not result in a significant decrease in relative misfit values. Although the calculated age peak at ~ 4.4 Ma is represented by only one zircon grain in the CP dacite, it is also observed in the MG zircons as a main sub-group. The significance of the age peak at ~ 4.8 Ma is uncertain, since it is represented only by one MG zircon grain. This indicates at least four major episodes of zircon growth (at ~ 3.3, 3.7, 4.1, and 4.4 Ma, Fig. 3) in the Tschicoma magmatic systems. Core and rim age differences in individual zircon grains almost cover the full age range recorded in each sample, from within analytical uncertainties to over 700 kyr (Fig. 4). Sector or oscillatory zoned zircons without notable resorption feature normally have small core-rim age differences (< 310 kyr). In zircons with a resorption texture, cores are commonly > 330 kyr older than corresponding rims. Resorbed old zircon cores clearly resulted from dissolution via heating and/or change to zircon-undersaturated melt compositions, indicating incorporation of pre-existing zircon from earlier emplaced intrusions during Tschicoma activity. The zircon grains with the largest core-rim age difference (~ 700 kyr) in both MG (grain no. 4; Fig. 2) and CP (grain no. 19; Fig. 2) samples have a ~ 4.4 Ma resorbed core and a ~ 3.7 Ma rim, which correspond to two major episodes of zircon growth. The ~ 4.4 Ma cores, once formed, likely were stored for ~ 700 kyr before they went through a dissolution–recrystallization-storage process at ~ 3.7 Ma. Afterwards, the CP zircon grain was stored for another ~ 500 kyr before a second rejuvenating event that led to eruption at ~ 3.2 Ma. The MG zircon grain was only stored for another ~ 100 kyr before the eruption event at ~ 3.6 Ma. Magma can be stored at near-solidus temperatures during most of its lifespan before rapid remobilization (e.g., Cooper and Kent 2014). Numerical modelling by Calogero et al. (2020) shows that at elevated crustal ambient temperatures (> 600 °C), regional partial melting surrounding any emplaced magmas from depth can persist on the order of thousands of years with the potential to solidify again, depending on the volume of magma emplaced. Calculated zircon crystallization temperatures ($T_{\text{Ti-in-zircon}}$) are centered at ~ 730 °C (Fig. 5b). MELTS modelling (Gualda and Ghiorso 2015) shows that the Tschicoma magma represented by the MG and CP whole-rock compositions at such a low temperature should be mushy, containing > 60% crystals (assuming a pressure of 238 MPa and oxygen fugacity at NNO + 1.3, where NNO is the nickel–nickel oxide fO_2 buffer, Wu et al. 2020). Therefore, the Tschicoma antecrystic zircons and their host magma pockets likely experienced long-term storage at near-solidus or even sub-solidus conditions punctured by large heating–cooling events. Major zircon growth events are more likely to have occurred episodically every 300–400 kyr in response to pulsed magma recharge that caused periodical temperature and/or composition fluctuations in the magma reservoir.

Despite pulses in growth rates, overall continuous zircon crystallization ages suggest the presence of zircon-saturated melts continuously over one million years, indicating frequent small magma recharge and cooling events in between the major events. Zircon recycling and crystallization followed by storage must have occurred contemporaneously over most of the protracted magma history, given the largely overlapped age range between cores and rims (Fig. 3a, b, d and e). The different zircon crystallization or dissolution histories imply their residence within different parts of the Tschicoma reservoir. Zircons formed during a single major growth period normally show large compositional variations including zircon-derived $\delta^{18}O_{\text{melt}}$, $T_{\text{Ti-in-zircon}}$, U, Zr/Hf, and Eu_N/Eu^* (Fig. 5) favouring zircon growth in separate melt lenses with different compositions. Individual zircon-saturated melt lenses had

been forming and cooling in an upper crustal mush zone throughout its lifespan, potentially resulting from magma recharge/intrusion at varying locations through time. Such melt lenses developed more extensively during each major zircon growth events. The hotter, less-evolved recharge magma can partially melt its surrounding older intrusions (at near-solidus or even sub-solidus conditions) and mix with the resulting melts and crystal cargo (e.g., Hughes et al. 2021), causing dissolution of the pre-existing zircons. The hybrid magma may go through a cooling process during which zircon regrowth occurs. We assume a temperature of 905 °C (calculated from the high-Al amphiboles that crystallized during/after magma recharge/mixing in the mush zone; Wu et al. 2020) for the hybrid magma, and its composition is approximated by the MG and CP whole-rock data. Zirconium concentration in the magma is 524–836 ppm Zr below saturation, depending on different zircon saturation models (e.g., Watson and Harrison 1983 or Boehnke et al. 2013). Dissolution calculations based on Eq. 17 of Watson (1996) suggest that it takes 1200–1800 years to completely dissolve a zircon crystal with a radius of 157 μm (average half-length of MG and CP zircons). It takes 500–1200 years to reduce such a zircon to the size of the two resorbed zircon cores discussed earlier (radius of 120 and 88 μm, respectively, for MG grain no.4 and CP grain no.19), which is the maximum time for the heating process during the major recharge event at ~ 3.7 Ma. Although MG and CP zircons are not in a spherical geometry, the calculated dissolution timescales should be valid in the order of magnitude. The heating periods during more frequent smaller recharge events should be shorter and on the order of hundreds of years. Preservation of antecrystic zircons covering an age span of ~ 1 Myr suggests that the recharge-induced melting/mixing-recrystallization-storage cycle repeated frequently in different parts of the large mush zone, and each melting stage may have lasted for several hundred to more than a thousand years (< 500–1200 years). Zircons crystallized and were stored at temperatures significantly lower than those calculated from low-Al amphiboles (815 ± 16 °C, 1σ) from the Tschicoma silicic mush zone (Wu et al. 2020). The presence of low-*T* zircon in higher-*T* liquid requires either unlocking of crystal mush by heating, or mixing of near-minimum rhyolitic melt with mafic magma to produce dacite. The ubiquitous rounded zircon surfaces resulting from dissolution also indicate residence in zircon-undersaturated melt before eruption, and may be indicative of thermal events not represented by Ti-in-zircon thermometry which only preserves conditions of zircon saturation. Separate melts lenses were connected during such pre-eruption remobilization, producing the complex crystal population seen in each eruption.

Evolution of the Tschicoma magmatic systems

Forming andesitic and dacitic magmas at polygenetic centers often involves magma mixing and mingling (Walker et al. 2010; Kent et al. 2010; Fodor and Johnson 2016), which are commonly recorded in disequilibrium mineral textures and occurrence of mafic enclaves (e.g., Crater Lake, Bacon and Lanphere 2006). Evidence for magma mixing in Tschicoma dacites from the northern JMVF has been documented in previous studies, which includes the existence of basaltic andesite enclaves, whole-rock chemical modelling (Rowe et al. 2007), disequilibrium mineral textures, and coexistence of multiple mineral populations (Wu et al. 2020). Negative Eu anomalies (Eu_N/Eu^*) and decreasing Zr/Hf mainly result from fractional crystallization of feldspar and zircon, respectively, since feldspar preferentially incorporates Eu, and zircon has larger partition coefficients for Zr than Hf (Claiborne et al. 2006). Therefore, zircon Eu_N/Eu^* and Zr/Hf ratio can serve as fractionation index for its host melt (Schmitt et al. 2017). Zr/Hf ratios do not show consistent variation patterns with age or from core to rim, but rim-ward decrease in Zr/Hf is more frequently observed (in 16 out of 27 zircon core–rim pairs; Figs. 5h and 6). A broad trend of increasing Eu_N/Eu^* (with a consistent rim-ward increase; 11 out of 18 pairs) toward younger zircon in Tschicoma samples (Figs. 5j and 6i) instead reflects zircon crystallization from less and less fractionated melt, consistent with magma recharge and mixing. Zircon chemical diversity is less obvious in the CP dacite. Compositional diversity in zircon host melt is also shown from zircon U, Sr, Y + REE, Nb, Th/U, and $(Dy/Yb)_N$ (Fig. 5c–g and i). Compared to the younger CP zircons, Y + REE and Nb concentrations are more scattered in the older MG zircons. No consistent compositional variations are observed from core to rim, but rim-ward decreases are predominant in Y + REE (20 out of 27 zircon core–rim pairs) and Nb (17 out of 27 pairs) (Fig. 6e and f).

Zircon crystallization temperatures based on Ti concentration (uncertainty of 30–41 °C; Ferry and Watson 2007) do not show any discernible pattern, and both rim-ward decrease and increase in temperatures are calculated (Figs. 5b and 6b). The variation of temperature through time does not show apparent thermal spikes corresponding to the four episodes of major zircon growth events (Fig. 5b). This is not surprising given that Ti-in-zircon thermometry only records magma temperatures that drop below zircon saturation. This limitation of using only zircon temperature-age distributions to decipher thermal history is recognized (Kent and Cooper 2018).

Regardless of the large variations in trace elements, rim-ward increase in zircon-derived $\delta^{18}O_{melt}$ is observed in 17 out of 25 zircon core-rim pairs (Figs. 5a and 6a). Based on a textural and chemical (major and trace elements) study of plagioclase and amphibole from Tschicoma dacites, Wu

et al. (2020) proposed mixing between an upper crustal silicic mush and recharging mafic magma. The O-isotopic composition of the silicic mush can be approximated by the Bearhead Rhyolite (zircon-derived $\delta^{18}O_{melt}$ range of 6.71–7.96‰ with a weighted average of 7.37 ± 0.10‰, 1σ; data from Wu et al. 2021); the Tschicoma silicic mush and the Bearhead magmatic system may have been sourced from the same partial melts derived from mid-crustal material given their chemically similar low-Ca plagioclase and low-Al amphibole (Wu et al. 2020). The recharging mafic magma is compositionally and isotopically similar to the Paliza Canyon rocks, and thus, its O-isotopic composition can be approximated by a low-Si Paliza Canyon dacite with zircon-derived $\delta^{18}O_{melt}$ range of 5.93–7.15‰ (weighted average of 6.45 ± 0.08‰, 1σ; data from Wu et al. 2021). This range extends above the normal-$\delta^{18}O$ range, consistent with assimilating crustal components (Wolff et al. 2005; Rowe et al. 2007) that are enriched in $\delta^{18}O$. If Tschicoma zircon crystals recorded the same mixing history, the rims formed in the hybrid magma should have $\delta^{18}O_{melt}$ comparable to the Paliza Canyon magma (mafic melt), and the cores to the Bearhead Rhyolite. The $\delta^{18}O_{melt}$ range between Tschicoma zircon rims and Paliza Canyon zircon is almost identical. Although a range of the Tschicoma zircon cores have $\delta^{18}O_{melt}$ values similar to the Bearhead rhyolite, more than half of the cores have lower $\delta^{18}O_{melt}$ values, either comparable to or even lower than Paliza Canyon magma; two cores are at the lower limit for normal-$\delta^{18}O$ range (e.g., mantle basalt value of 5.8 ± 0.2‰) and one core is within low-$\delta^{18}O$ magma range. To produce these low-$\delta^{18}O_{melt}$ Tschicoma zircon cores, the initial crustal-derived high-$\delta^{18}O$ melt, assumed to be represented by the Bearhead Rhyolite, must have exchanged O-isotopes with low-$\delta^{18}O$ component such as hydrothermally altered upper crust. In the JMVF, pre-Tschicoma hydrothermal systems developed at ~ 8 Ma and during the waning stage of Bearhead volcanism (7–6 Ma; WoldeGabriel and Goff 1989; Goff et al. 1992), which spatially overlaps the Tschicoma volcanics in the northern JMVF (Kelley et al. 2013). Assimilating hydrothermally altered crust probably was associated with the earlier shallow Bearhead magma reservoir (Justet and Spell 2001). This is consistent with the geographic location of the two samples; the south MG dacite is closer to the Bearhead system than the north CP dacite, and recorded the lowest calculated $\delta^{18}O_{melt}$ values in its zircon cores.

A 0.5 Myr lull (6–5.5 Ma) in volcanic activity between the Bearhead and Tschicoma volcanism corresponded to reduced tectonic activity. Renewed local extension was characterized by eastward shift of rift-bounding faults from the Cañada de Cochiti fault zone to the Pajarito fault zone at 5–4 Ma (Fig. 1; Gardner and Goff 1984). Such change in fault activity might be an essential control on the location of magma storage and magma–crust interaction during Tschicoma activity. The Tschicoma magma reservoir is located between the two major fault zones (Fig. 1), where mid-crustal extensional structures could have been created during the eastward tectonic shift. Such structures served as conduits controlling the location of magma emplacement and storage in the upper crust. Development of such a large hybrid silicic magma reservoir in turn may also have promoted the eastward shift of the major fault zone (Gardner and Goff 1984).

Compositions of melts in equilibrium with zircon can be calculated based on partition coefficients reported by Sano et al. (2002), based on compositional similarities. Zircon-derived melts show larger variations in rare-earth elements (REE), compared to the whole-rock data of Tschicoma lavas from northeast JMVF (Fig. 7). When normalized to chondrite values, zircon-derived melts (for both samples) and whole-rocks both have light rare-earth element (LREE) enriched patterns. Melts calculated from most zircon cores and almost all rims are slightly depleted in middle rare-earth elements (MREE) compared to heavy rare-earth elements (HREE). Propagation of 1σ error on partitioning data shifts calculated equilibrium melt compositions slightly, but overall trends and differences between core and rim populations are preserved (Supplementary Fig. S3). Similar to the diversity in zircon-derived melt compositions, calculated melt Sr, Ba, La, and Ce based on plagioclase compositions also show much larger variations than whole-rock data (Wu et al. 2020), suggesting that the complex growth records of crystal cargos are often erased during whole-rock analyses. Coexistence of two groups of both plagioclase (An-poor core and An-rich rim) and amphibole (low-Al low-temperature and high-Al high-temperature) in Tschicoma dacites shown by Wu et al. (2020) suggests that the compositionally more evolved crystal groups were recycled from an upper crustal silicic mush and the less-evolved populations were crystallized during or after mixing with more primitive recharge magmas. Crystal recycling is consistent with prolonged zircon crystallization and resorption textures. The REE compositions of melts in equilibrium with Tschicoma amphiboles are also calculated based on partition coefficients from Nandedkar et al. (2016) to be compared directly with those calculated from zircons (amphibole REE data from Wu et al. 2020). Melts calculated from both high-Al and low-Al amphiboles also have LREE-enriched patterns that are similar to melts calculated from zircon (Fig. 7). Whole-rock data do not show obvious Eu anomalies (0.90–1.00). High-Al amphibole-derived melts have large variations in Eu anomalies (0.59–1.41), and low-Al amphibole-derived melts have consistent negative Eu anomalies (0.43–0.81) and higher REE concentrations (Figs. 7 and 8). Compared to melts derived from amphibole, zircon-derived melts show a similar range of Eu anomalies (0.36–1.53; Fig. 8). Negative Eu anomalies suggest zircon and amphibole co-crystallized

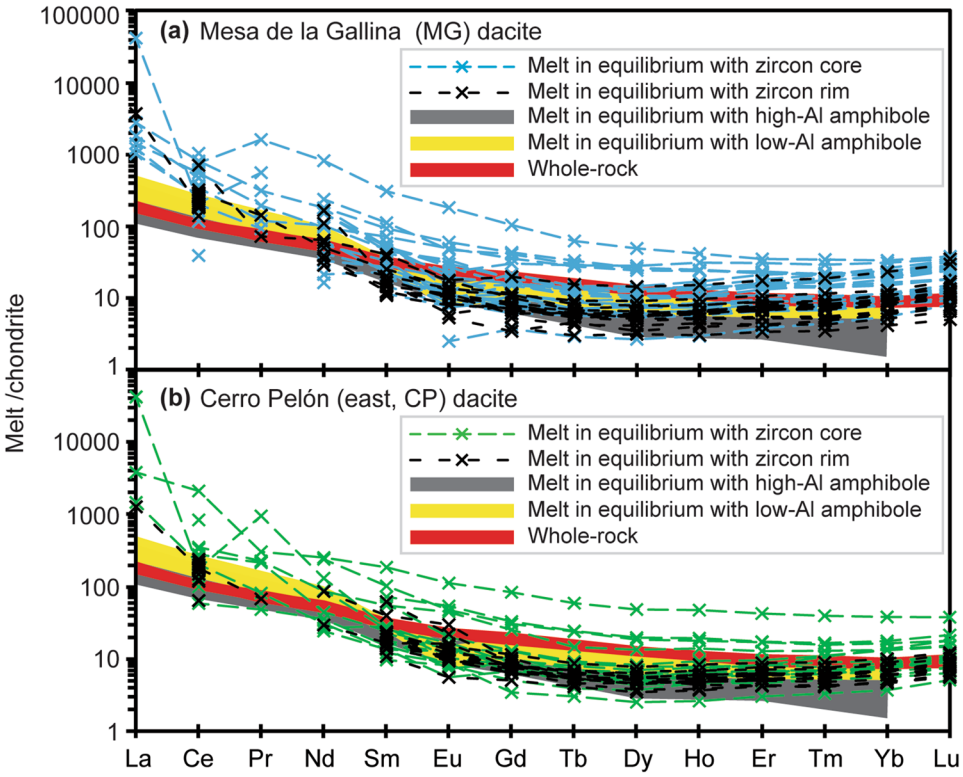

Fig. 7 Chondrite normalized rare-earth elements (REE) patterns for melts calculated from zircons in the Mesa de la Gallina dacite (**a**) and Cerro Pelón (east) dacite (**b**). Whole-rock data and amphibole-derived melt compositions are also shown for comparison (data from Rowe et al. 2007 and Wu et al. 2020). Chondrite values after Sun and McDonough (1989)

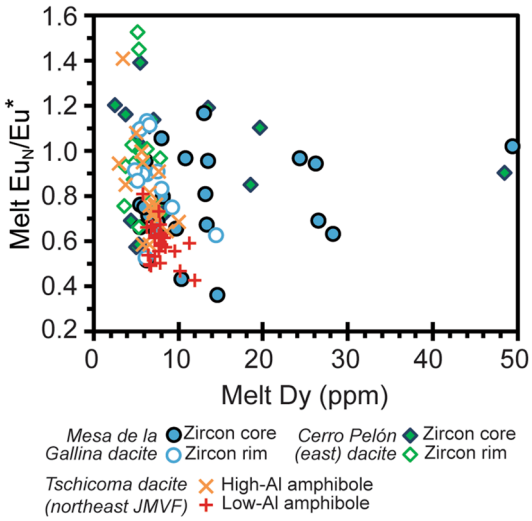

Fig. 8 Eu_N/Eu^* vs Dy plot for melts calculated from Tschicoma zircon and amphibole. 2σ error bars are smaller than the symbols and thus are not shown

with feldspar. Weak and positive Eu anomalies are evidence for recycling and dissolution of feldspar into magma or mixing with more mafic magma. This is consistent with major zircon growth events every 300–400 kyr from heating by recharge magma and subsequent cooling. Such periodic large magma recharge events (along with smaller events that had persisted in between) might be essential to thermally maintain the upper crustal mush and chemically modify the magmatic systems. Gradual thermal and chemical maturation of the Tschicoma magmatic systems is reflected by lower proportions of older antecrystic zircons (Fig. 3) and less chemical variations (e.g., Y + REE and Nb) in zircons from the younger CP dacite, which probably results from more efficient dissolution of pre-existing zircons. Under such conditions, elevated magma supply from depth at the end of the period of Tschicoma volcanism remelted pre-existing mush and combined isolated melt lenses into a single supersized magma chamber to produce the Bandelier Tuff (Rowe et al. 2007; Wolff and Ramos 2014; Wu et al. 2021). This transition marked the change from lower magnitude effusive individual dacitic eruptions into a rhyolitic supereruption.

Magma supply rates in long-lived magmatic system

Geochemical modelling suggests that the Tschicoma magmatic system was constructed of a series of melt lenses, identified by compositional and age variations. Magma supply rates are inherently important to maintaining the thermal structure of the transcrustal magmatic plumbing system and the development of individual melt lenses (Takada 1999). In the JMVF, the average eruption rate decreases from the early stage of volcanism (0.25 km^3/kyr during ~ 10–6 Ma) to Tschicoma activity (0.14 km^3/kyr during 5.5–2 Ma; Gardner et al. 1986; Kelley et al. 2013). Such reduced volcanic output may partly be attributed to

retaining more magmas in the middle-lower crustal levels, as the JMVF magmatic systems evolved toward shallower crustal levels (based on two-pyroxene barometry; Wu et al. 2020). More likely, this reflects a decrease in magma supply rate (e.g., Grunder et al. 2008). Here, we define magma supply rate as magma volume supplied from lower crust over a period of time, which may cool down as intrusions or erupt along with other magmas. We assume that the magma supply rate is proportional to magma eruption rate, that can be more accurately calculated (Grunder et al. 2008). Assuming a minimum plutonic:volcanic ratio of 4:1 (a common range is between 4:1 and 16:1 for silicic systems, de Silva and Gosnold 2007) during the Tschicoma volcanism, the minimum magma supply rate during Tschicoma activity is 0.7 km^3/kyr. Considering recharge events occurring every 300–400 kyr during Tschicoma activity, this rate suggests one cycle of large magma recharge and subsequent smaller events may have contributed as much as 210–280 km^3 magma to the silicic mush zone. The earlier intermediate-silicic magmas (Paliza Canyon low-Si dacite, La Grulla high-Si andesite, and Bearhead rhyolite) erupted during ~ 10–6 Ma, have unimodal zircon age distributions, and do not contain antecrystic zircons from earlier intrusions (Wu et al. 2021), which might be a result of effectively thermal resetting of pre-existing zircon due to high magma supply rate. It is noteworthy that although separate melts saturated in zircon periodically existed over one million years during Tschicoma activity, unlike the Otowi Member of the Bandelier Tuff that preserved zircons derived from earlier periods of magmatism including the Paliza Canyon (10–7 Ma), Bearhead (7–6 Ma), and Tschicoma (5.5–2 Ma), as well as Proterozoic basement (Wu et al. 2021), the Tschicoma lavas do not show any zircon inheritance from the older plutons (> 6 Ma) and the basement rock. The lack of Bearhead and Paliza Canyon zircons may indicate that the JMVF pre-caldera magmatism occurred in separate domains (Wu et al. 2021). The Tschicoma melt lenses were likely effectively shielded from pristine Proterozoic basement rocks by the surrounding mush zone, as proposed for the San Juan volcanic field (e.g., Riciputi et al. 1995), which explains the absence of inherited Proterozoic zircons. Preservation of the large spread of zircon age distribution in Tschicoma dacites is likely enhanced by two conditions. First, the Tschicoma systems are located in upper crust that was thermally (and also chemically) modified over a few million years' earlier magmatism (~ 10–6 Ma) and thus capable of accommodating low-temperature crystal mush over a long time. Second, the long-term magma supply rate is low enough not to cause widespread zircon dissolution, but more importantly high enough to keep the whole system 'alive', i.e., above the petrologic solidus. For example, the absence of older zircons in the Tshirege Member of the Bandelier Tuff is attributed to efficient thermal dissolution of zircons in the relic Otowi mush due to a high rate of magma supply (Wu et al. 2021). Many long-lived plutons (e.g., Spirit Mountain batholith, Walker et al. 2007) may represent a different fate of such a system when magma supply rates were too low. The Aucanquilcha volcanic cluster in the Andes of northern Chile (AVC, Walker et al. 2010, 2013) is a comparable long-lived intermediate-to-silicic continental volcanic field to the Tschicoma Formation magmatic systems. Both volcanic fields show ~ 10 Myr magmatic evolution from diverse intermediate compositions to more homogenous dacite (Walker et al. 2013). Walker et al. (2013) also envisioned the Aucanquilcha subvolcanic reservoir as patchworks of separate magma chambers and crystal mushes, consistent with our explanation of the Tschicoma subvolcanic systems. Both systems show prolonged zircon crystallization over timescales of million years with periodic magma recharge (Walker et al. 2010).

In the AVC, the early two stages of activity show an increase in eruption rate from ~ 0.013 km^3/kyr (~ 11–8 Ma) to 0.027 km^3/kyr (~ 6–4 Ma). Output rate during the subsequent peak stage (~ 4–2 Ma) reaches a maximum of 0.077 km^3/kyr, which is followed by a sharp decrease to 0.04 km^3/kyr in the recent waning stage since 1 Ma (Grunder et al. 2008). The overall volcanic output in AVC (0.03 km^3/kyr, Grunder et al. 2008) is significantly lower than that of the JMVF pre-caldera stage (10–2 Ma, 0.19 km^3/kyr), reflected by erupted volumes (325 vs 1500 km^3). This suggests that smaller magmatic systems can be sustained at relatively lower magma supply rate. Nonetheless, an almost 50% decrease in magma eruption rate from the peak to the recent stage in AVC is similar to the decrease in output rate from the early stage to the Tschicoma volcanism in the JMVF. It is worth noting that magma output rates at AVC and JMVF (pre-caldera stage) are above the lower limit (< 0.01 km^3/kyr) of the eruption rates for intermediate-to-silicic magma from the global compilation of White et al. (2006), but are 1–2 orders of magnitude lower than their calculated average values (2.3–4 km^3/kyr). The recent AVC volcanism (since 1 Ma) also has zircon age distributions spreading over 1 Myr, in contrast to the restricted zircon age range (less than 500 kyr) during the 4–~ 2 Ma peak stage of AVC volcanism, which is explained by pervasive dissolution of antecrystic zircons during the period of elevated magma output (also supply) rate (Walker et al. 2010). However, the fate of the two volcanic fields looks to be totally different, potentially controlled by changing magma supply rates. The Tschicoma Formation magmatic system culminates in the formation of the super-scale rhyolitic Bandelier magmatic system, whereas the comparable AVC dacite-dominant magmatic system is in a waning stage, likely to cease activity (Grunder et al. 2008).

Conclusions

The dacite-dominant Tschicoma Formation in the JMVF represents effusive and dome-forming eruptions from long-lived magmatic systems during 5.5–2 Ma. Zircons from two separate Tschicoma eruptions both have large and continuous age spectra (0.84–1.08 Myr). Individual zircon grains also show core-rim age differences up to 720–740 kyr, comparable to the whole zircon age range. Zircon age variations in both lavas far exceed analytical uncertainties (56–160 kyr, 1σ), and thus indicate a complex history of zircon growth including recycling of antecrystic zircon, supported by resorption texture in zircon cores. Presence of zircon-saturated melts and thus zircon growth occurred throughout the whole prolonged magmatic history, but major growth likely happened episodically as at least four pulses as indicated by unmixing calculations of the U–Pb ages; contemporaneous zircon crystallization and dissolution indicate crystal residence in separate melt lenses during most of the pre-eruption history. Once crystallized, zircons were likely stored at near-solidus or even sub-solidus conditions, but could be remobilized by major magma recharge events every 300–400 kyr, and more frequent smaller events in between, that kept the long-lived silicic mush zone alive. Each period of heating/mixing may last for several hundred to more than a thousand years (< 500–1200 years) before cooling-induced crystallization and storage. Complexities in both zircon U–Pb age and chemistry suggest the Tschicoma subvolcanic systems are likely to be patchworks consisting of isolated melt lenses and crystal mush, and each eruption may tap multiple lenses introduced by pre-eruption magma recharge, consistent with other dacitic systems such as those seen in the AVC. Less chemical diversity and a lower proportion of old zircon in the younger Tschicoma dacite imply gradual chemical and thermal maturation of the volcanic field, which eventually led to the supersized Bandelier magmatic system. When compared with other long-lived intermediate-to-silicic magmatic systems, incremental growth of magma reservoirs involving mingling with and recycling of precursor plutons over million years timescales is likely common. Magma supply rate is an essential control on the fate of such long-lived mushy magmatic systems; its fluctuation may either introduce large-scale partial melting leading to a caldera-forming silicic magma chamber, or terminate the magmatic system.

Supplementary Information The online version contains supplementary material available at https://doi.org/10.1007/s00410-022-01930-9.

Acknowledgements We acknowledge technical support from William Phillips, Natalia Abrego, David Wackrow, Andrew Canada, Kirsty Vincent, David Flynn, and Andres Arcila-Rivera with sample preparations, and Scott Boroughs and Stuart Morrow with analyses. We thank Mark Fanning for both preparation of zircon mounts and help with zircon U–Pb dating. We appreciate the editorial handling by Editor Gordon Moore and constructive reviews by Laura Waters, Meredith Calogero, and an anonymous reviewer.

Funding Open Access funding enabled and organized by CAUL and its Member Institutions. This research was supported by the MBIE Resilience to Nature's Challenges, Volcanic Hazards Theme (to S.J.C.), University of Auckland School of Environment PBRF funds and R&SL support (to M.C.R.), as well as University of Auckland PReSS account and China Scholarship Council scholarship (no. 201506400051; to J.W.). J.W. and S.J.C. acknowledge support of the Transitioning Taranaki to a Volcanic Future MBIE Endeavour Research Program (UOAX1913).

References

Aldrich MJ (1986) Tectonics of the Jemez lineament in the Jemez Mountains and Rio Grande rift. J Geophys Res-Solid Earth 91:1753–1762. https://doi.org/10.1029/JB091iB02p01753

Bachmann O, Bergantz GW (2004) On the origin of crystal-poor rhyolites: extracted from batholithic crystal mushes. J Petrol 45:1565–1582. https://doi.org/10.1093/petrology/egh019

Bacon CR, Lanphere MA (2006) Eruptive history and geochronology of Mount Mazama and the Crater Lake region, Oregon. Geol Soc Am Bull 118:1331–1359. https://doi.org/10.1130/B25906.1

Bindeman IN, Ponomareva VV, Bailey JC, Valley JW (2004) Volcanic arc of Kamchatka: a province with high-$\delta^{18}O$ magma sources and large-scale $^{18}O/^{16}O$ depletion of the upper crust. Geochim Cosmochim Acta 68:841–865. https://doi.org/10.1016/j.gca.2003.07.009

Bindeman IN, Schmitt AK, Valley JW (2006) U-Pb zircon geochronology of silicic tuffs from the Timber Mountain/Oasis Valley caldera complex, Nevada: rapid generation of large volume magmas by shallow-level remelting. Contrib Mineral Petrol 152:649–665. https://doi.org/10.1007/s00410-006-0124-1

Black LP, Kamo SL, Allen CM, Davis DW, Aleinikoff JN, Valley JW, Mundil R, Campbell IH, Korsch RJ, Williams IS, Foudoulis C (2004) Improved $^{206}Pb/^{238}U$ microprobe geochronology by the monitoring of a trace-element-related matrix effect; SHRIMP, ID-TIMS, ELA-ICP-MS and oxygen isotope documentation for a series of zircon standards. Chem Geol 205:115–140. https://doi.org/10.1016/j.chemgeo.2004.01.003

Boehnke P, Watson EB, Trail D, Harrison TM, Schmitt AK (2013) Zircon saturation re-revisited. Chem Geol 351:324–334. https://doi.org/10.1016/j.chemgeo.2013.05.028

Brookins DG, Laughlin AW (1983) Rb–Sr geochronologic investigation of precambrian samples from deep geothermal drill holes, Fenton Hill, New Mexico. J Volcanol Geotherm Res 15:43–58. https://doi.org/10.1016/0377-0273(83)90095-1

Brown SJA, Fletcher IR (1999) SHRIMP U–Pb dating of the preeruption growth history of zircons from the 340 ka Whakamaru Ignimbrite, New Zealand: evidence for > 250 k.y. magma residence times. Geology 27:1035–1038. https://doi.org/10.1130/0091-7613(1999)027%3C1035:SUPDOT%3E2.3.CO;2

Calogero MA, Hetland EA, Lange RA (2020) High-resolution numerical modeling of heat and volatile transfer from basalt to wall rock: application to the crustal column beneath Long Valley caldera, CA. J Geophys Res-Solid Earth 125:e2018JB016773. https://doi.org/10.1029/2018JB016773

Cashman KV, Sparks RSJ, Blundy JD (2017) Vertically extensive and unstable magmatic systems: a unified view of igneous processes. Science 355:eaag3055. https://doi.org/10.1126/science.aag3055

Cherniak DJ, Watson EB (2001) Pb diffusion in zircon. Chem Geol 172:5–24. https://doi.org/10.1016/S0009-2541(00)00233-3

Claiborne LL, Miller C, Walker B, Wooden J, Mazdab F, Bea F (2006) Tracking magmatic processes through Zr/Hf ratios in rocks and Hf and Ti zoning in zircons: an example from the Spirit Mountain batholith, Nevada. Mineral Mag 70:517–543. https://doi.org/10.1180/0026461067050348

Cook GW, Wolff JA, Self S (2016) Estimating the eruptive volume of a large pyroclastic body: the Otowi Member of the Bandelier Tuff, Valles caldera, New Mexico. Bull Volcanol 78:10. https://doi.org/10.1007/s00445-016-1000-0

Cooper KM, Kent AJR (2014) Rapid remobilization of magmatic crystals kept in cold storage. Nature 506:480–483. https://doi.org/10.1038/nature12991

Coutts DS, Matthews WA, Hubbard SM (2019) Assessment of widely used methods to derive depositional ages from detrital zircon populations. Geosci Front 10:1421–1435. https://doi.org/10.1016/j.gsf.2018.11.002

de Silva SL, Gosnold WD (2007) Episodic construction of batholiths: insights from the spatiotemporal development of an ignimbrite flare-up. J Volcanol Geotherm Res 167:320–335. https://doi.org/10.1016/j.jvolgeores.2007.07.015

Ferry JM, Watson EB (2007) New thermodynamic models and revised calibrations for the Ti-in-zircon and Zr-in-rutile thermometers. Contrib Mineral Petrol 154:429–437. https://doi.org/10.1007/s00410-007-0201-0

Fodor RV, Johnson KG (2016) Origin of Miocene andesite and dacite in the Goldfield-Superstition volcanic province, central Arizona: hybrids of mafic and silicic magma mixing. Geochim Cosmochim Acta 185:394–417. https://doi.org/10.1016/j.gca.2016.04.001

Fu B, Bröcker M, Ireland T, Holden P, Kinsley LPJ (2015) Zircon U–Pb, O, and Hf isotopic constraints on Mesozoic magmatism in the Cyclades, Aegean Sea, Greece. Int J Earth Sci 104:75–87. https://doi.org/10.1007/s00531-014-1064-z

Gardner JN, Goff FE (1984) Potassium-argon dates from the Jemez volcanic field: Implications for tectonic activity in the north-central Rio Grande Rift. In: Baldridge WS, Dickerson PW, Riecker RE, Zidek J (eds) Rio Grande Rift (Northern New Mexico). New Mexico Geological Society 35th Annual Fall Field Conference Guidebook, pp 75–81

Gardner JN, Goff F, Garcia S, Hagan RC (1986) Stratigraphic relations and lithologic variations in the Jemez volcanic field, New Mexico. J Geophys Res-Solid Earth 91:1763–1778. https://doi.org/10.1029/JB091iB02p01763

Gardner JN, Goff F, Kelley S, Jacobs E (2010) Rhyolites and associated deposits of the Valles-Toledo caldera complex. New Mex Geol 32:3–18

Goff F, Gardner J, Baldridge WS, Hulen J, Nielson D, Vaniman D, Heiken G, Dungan M, Broxton D (1989) Volcanic and hydrothermal evolution of Valles caldera and Jemez volcanic field: Field Excursion 17B. New Mexico Bur Min Miner Resour Mem 46:381–434

Goff F, Gardner JN, Hulen JB, Nielson DL, Charles R, WoldeGabriel G, Vuataz F-D, Musgrave JA, Shevenell L, Kennedy BM (1992) The Valles caldera hydrothermal system, past and present, New Mexico, USA. Sci Drill 3:181–204

Goff F, Warren RG, Goff CJ, Dunbar N (2014) Eruption of reverse-zoned upper Tshirege Member, Bandelier Tuff from centralized vents within Valles caldera, New Mexico. J Volcanol Geotherm Res 276:82–104. https://doi.org/10.1016/j.jvolgeores.2014.02.018

Grunder AL, Klemetti EW, Feeley TC, McKee CM (2008) Eleven million years of arc volcanism at the Aucanquilcha Volcanic Cluster, northern Chilean Andes: implications for the life span and emplacement of plutons. Earth Environ Sci Trans R Soc Edinb 97:415–436

Gualda GA, Ghiorso MS (2015) MELTS_Excel: a Microsoft Excel-based MELTS interface for research and teaching of magma properties and evolution. Geochem Geophys Geosyst 16:315–324. https://doi.org/10.1002/2014GC005545

Hawkesworth CJ, Kemp AIS (2006) Using hafnium and oxygen isotopes in zircons to unravel the record of crustal evolution. Chem Geol 226:144–162. https://doi.org/10.1016/j.chemgeo.2005.09.018

Hou T, Botcharnikov R, Moulas E, Just T, Berndt J, Koepke J, Zhang Z, Wang M, Yang Z, Holtz F (2020) Kinetics of Fe–Ti oxide re-equilibration in magmatic systems: implications for thermo-oxybarometry. J Petrol 61:egaa116. https://doi.org/10.1093/petrology/egaa116

Hughes GE, Petrone CM, Downes H, Varley NR, Hammond SJ (2021) Mush remobilisation and mafic recharge: A study of the crystal cargo of the 2013–17 eruption at Volcán de Colima, Mexico. J Volcanol Geotherm Res 416:107296. https://doi.org/10.1016/j.jvolgeores.2021.107296

Jochum KP, Nohl U, Herwig K, Lammel E, Stoll B, Hofmann AW (2005) GeoReM: a new geochemical database for reference materials and isotopic standards. Geostand Geoanal Res 29:333–338. https://doi.org/10.1111/j.1751-908X.2005.tb00904.x

Justet L, Spell TL (2001) Effusive eruptions from a large silicic magma chamber: the Bearhead Rhyolite, Jemez volcanic field, NM. J Volcanol Geotherm Res 107:241–264. https://doi.org/10.1016/S0377-0273(00)00296-1

Kaiser JF (2014) Understanding large resurgent calderas and associated magma systems: the Pastos Grandes Caldera Complex, southwest Bolivia. Dissertation, Oregon State University

Kaiser JF, de Silva S, Schmitt AK, Economos R, Sunagua M (2017) Million-year melt–presence in monotonous intermediate magma for a volcanic–plutonic assemblage in the Central Andes: contrasting histories of crystal-rich and crystal-poor super-sized silicic magmas. Earth Planet Sci Lett 457:73–86. https://doi.org/10.1016/j.epsl.2016.09.048

Karakas O, Dufek J (2015) Melt evolution and residence in extending crust: thermal modeling of the crust and crustal magmas. Earth Planet Sci Lett 425:131–144. https://doi.org/10.1016/j.epsl.2015.06.001

Karlstrom KE, CD-ROM Working Group (2002) Structure and evolution of the lithosphere beneath the Rocky Mountains: initial results from the CD-ROM experiment. GSA Today 12:4–10

Kelley SA, McIntosh WC, Goff F, Kempter KA, Wolff JA, Esser R, Braschayko S, Love D, Gardner JN (2013) Spatial and temporal trends in pre-caldera Jemez Mountains volcanic and fault activity. Geosphere 9:614–646. https://doi.org/10.1130/GES00897.1

Kent AJR, Cooper KM (2018) How well do zircons record the thermal evolution of magmatic systems? Geology 46:111–114. https://doi.org/10.1130/G39690.1

Kent AJ, Darr C, Koleszar AM, Salisbury MJ, Cooper KM (2010) Preferential eruption of andesitic magmas through recharge filtering. Nat Geosci 3:631–636. https://doi.org/10.1038/NGEO924

Ludwig KR (2008) Isoplot/Ex version 3.75, a geochronological toolkit for Microsoft Excel, Berkeley Geochronology Center, Berkeley

Nandedkar RH, Hürlimann N, Ulmer P, Müntener O (2016) Amphibole-melt trace element partitioning of fractionating calc-alkaline magmas in the lower crust: an experimental study. Contrib Mineral Petrol 171:1–25. https://doi.org/10.1007/s00410-016-1278-0

Phillips EH, Goff F, Kyle PR, McIntosh WC, Dunbar NW, Gardner JN (2007) The $^{40}Ar/^{39}Ar$ age constraints on the duration of resurgence at the Valles caldera, New Mexico. J Geophys Res Solid Earth 112:B08201. https://doi.org/10.1029/2006JB004511

Qin T, Wu F, Wu Z, Huang F (2016) First-principles calculations of equilibrium fractionation of O and Si isotopes in quartz, albite, anorthite, and zircon. Contrib Mineral Petrol 171:91. https://doi.org/10.1007/s00410-016-1303-3

Reid MR, Vazquez JA (2017) Fitful and protracted magma assembly leading to a giant eruption, Youngest Toba Tuff, Indonesia. Geochem Geophys Geosyst 18:156–177. https://doi.org/10.1002/2016GC006641

Reid MR, Coath CD, Harrison TM, McKeegan KD (1997) Prolonged residence times for the youngest rhyolites associated with Long Valley Caldera: $^{230}Th–^{238}U$ ion microprobe dating of young zircons. Earth Planet Sci Lett 150:27–39. https://doi.org/10.1016/S0012-821X(97)00077-0

Riciputi LR, Johnson CM, Sawyer DA, Lipman PW (1995) Crustal and magmatic evolution in a large multicyclic caldera complex: isotopic evidence from the central San Juan volcanic field. J Volcanol Geotherm Res 67:1–28. https://doi.org/10.1016/0377-0273(94)00097-Z

Rowe MC, Wolff JA, Gardner JN, Ramos FC, Teasdale R, Heikoop CE (2007) Development of a continental volcanic field: petrogenesis of pre-caldera intermediate and silicic rocks and origin of the Bandelier magmas, Jemez Mountains (New Mexico, USA). J Petrol 48:2063–2091. https://doi.org/10.1093/petrology/egm050

Rubin AE, Cooper KM, Till CB, Kent AJR, Costa F, Bose M, Gravley D, Deering C, Cole J (2017) Rapid cooling and cold storage in a silicic magma reservoir recorded in individual crystals. Science 356:1154–1156. https://doi.org/10.1126/science.aam8720

Sambridge MS, Compston W (1994) Mixture modeling of multi-component datasets with application to ion probe zircon ages. Earth Planet Sci Lett 128:373–390. https://doi.org/10.1016/0012-821X(94)90157-0

Sano Y, Terada K, Fukuoka T (2002) High mass resolution ion microprobe analysis of rare earth elements in silicate glass, apatite and zircon: lack of matrix dependency. Chem Geol 184:217–230. https://doi.org/10.1016/S0009-2541(01)00366-7

Schärer U (1984) The effect of initial ^{230}Th disequilibrium on young U–Pb ages: the Makalu case, Himalaya. Earth Planet Sci Lett 67:191–204. https://doi.org/10.1016/0012-821X(84)90114-6

Schmitt AK, Klitzke M, Gerdes A, Schäfer C (2017) Zircon hafnium-oxygen isotope and trace element petrochronology of intraplate volcanic rocks from the Eifel (Germany) and implications for mantle versus crustal origins of zircon megacrysts. J Petrol 58:1841–1870. https://doi.org/10.1093/petrology/egx075

Shaw CA, Karlstrom KE (1999) The Yavapai–Mazatzal crustal boundary in the southern Rocky Mountains. Rocky Mt Geol 34:37–52. https://doi.org/10.2113/34.1.37

Siebel W, Schmitt AK, Danišík M, Chen F, Meier S, Weiß S, Eroğlu S (2009) Prolonged mantle residence of zircon xenocrysts from the western Eger rift. Nat Geosci 2:886. https://doi.org/10.1038/NGEO695

Smith RL, Bailey RA, Ross C (1970) Geologic map of the Jemez Mountains, New Mexico (No. 571)

Sun SS, McDonough W (1989) Chemical and isotopic systematics of oceanic basalts: implications for mantle composition and processes. Geol Soc Lond Spec Publ 42:313–345. https://doi.org/10.1144/GSL.SP.1989.042.01.19

Szymanowski D, Wotzlaw J-F, Ellis BS, Bachmann O, Guillong M, von Quadt A (2017) Protracted near-solidus storage and pre-eruptive rejuvenation of large magma reservoirs. Nat Geosci 10:777–782. https://doi.org/10.1038/NGEO3020

Szymanowski D, Ellis BS, Wotzlaw J-F, Bachmann O (2019) Maturation and rejuvenation of a silicic magma reservoir: high-resolution chronology of the Kneeling Nun Tuff. Earth Planet Sci Lett 510:103–115. https://doi.org/10.1016/j.epsl.2019.01.007

Takada A (1999) Variations in magma supply and magma partitioning: the role of tectonic settings. J Volcanol Geotherm Res 93:93–110. https://doi.org/10.1016/S0377-0273(99)00082-7

Tera F, Wasserburg G (1972) U–Th–Pb systematics in three Apollo 14 basalts and the problem of initial Pb in lunar rocks. Earth Planet Sci Lett 14:281–304. https://doi.org/10.1016/0012-821X(72)90128-8

Valley JW (2003) Oxygen isotopes in zircon. Rev Mineral Geochem 53:343–385. https://doi.org/10.2113/0530343

Walker BA, Miller CF, Claiborne LL, Wooden JL, Miller JS (2007) Geology and geochronology of the Spirit Mountain batholith, southern Nevada: implications for timescales and physical processes of batholith construction. J Volcanol Geotherm Res 167:239–262. https://doi.org/10.1016/j.jvolgeores.2006.12.008

Walker BA, Grunder AL, Wooden JL (2010) Organization and thermal maturation of long-lived arc systems: evidence from zircons at the Aucanquilcha volcanic cluster, northern Chile. Geology 38:1007–1010. https://doi.org/10.1130/G31226.1

Walker BA, Klemetti EW, Grunder AL, Dilles JH, Tepley FJ, Giles D (2013) Crystal reaming during the assembly, maturation, and waning of an eleven-million-year crustal magma cycle: thermobarometry of the Aucanquilcha Volcanic Cluster. Contrib Mineral Petrol 165:663–682. https://doi.org/10.1007/s00410-012-0829-2

Watson EB (1996) Dissolution, growth and survival of zircons during crustal fusion: kinetic principals, geological models and implications for isotopic inheritance. Trans R Soc Edinb-Earth Sci 87:43–56. https://doi.org/10.1017/S0263593300006465

Watson EB, Harrison TM (1983) Zircon saturation revisited: temperature and composition effects in a variety of crustal magma types. Earth Planet Sci Lett 64:295–304. https://doi.org/10.1016/0012-821X(83)90211-X

White SM, Crisp JA, Spera FJ (2006) Long-term volumetric eruption rates and magma budgets. Geochem Geophys Geosyste 7:Q03010. https://doi.org/10.1029/2005GC001002

Williams IS (1998) U–Th-Pb geochronology by ion microprobe. In: McKibben MA, Shanks III WC, Ridley WI (eds) Applications of microanalytical techniques to understanding mineralizing processes. Rev Econ Geol 7:1–35

WoldeGabriel G, Goff F (1989) Temporal relations of volcanism and hydrothermal systems in two areas of the Jemez volcanic field, New Mexico. Geology 17:986–989. https://doi.org/10.1130/0091-7613(1989)017%3C0986:TROVAH%3E2.3.CO;2

WoldeGabriel G, Naranjo AP, Fittipaldo MM (2007) Distribution, geochemistry, and correlation of Pliocene tephra in the Pajarito Plateau. Geol Jemez Region II: Guideb N M Geol Soc 58:275–283

Wolff JA, Ramos FC (2014) Processes in caldera-forming high-silica rhyolite magma: Rb–Sr and Pb isotope systematics of the Otowi Member of the Bandelier Tuff, Valles Caldera, New Mexico, USA. J Petrol 55:345–375. https://doi.org/10.1093/petrology/egt070

Wolff JA, Rowe MC, Teasdale R, Gardner JN, Ramos FC, Heikoop CE (2005) Petrogenesis of pre-caldera mafic lavas, Jemez Mountains volcanic field (New Mexico, USA). J Petrol 46:407–439. https://doi.org/10.1093/petrology/egh082

Wu J, Rowe MC, Cronin SJ, Wolff JA (2020) Mineralogical evidence of pre-caldera magma petrogenesis in the Jemez Mountains volcanic field, New Mexico, USA. J Petrol 7:egaa064. https://doi.org/10.1093/petrology/egaa064

Wu J, Cronin SJ, Rowe MC, Wolff JA, Barker SJ, Fu B, Boroughs S (2021) Crustal evolution leading to successive rhyolitic supereruptions in the Jemez Mountains volcanic field, New Mexico, USA. Lithos 396–397:106201. https://doi.org/10.1016/j.lithos.2021.106201